Journal of Colloid and Interface Science 606 (2022) 491–499

Contents lists available at ScienceDirect

Journal of Colloid and Interface Science

journal homepage: www.elsevier.com/locate/jcis

Photocatalytic overall water splitting without noble-metal: Decorating CoP on Al-doped $SrTiO_3$

Shichao Zong [1], Li Tian [1], Xiangjiu Guan *, Cheng Cheng, Jinwen Shi, Liejin Guo *

International Research Center for Renewable Energy (IRCRE), State Key Laboratory of Multiphase Flow in Power Engineering (MFPE), Xi'an Jiaotong University (XJTU), 28 West Xianning Road, Xi'an 710049, China

GRAPHICAL ABSTRACT

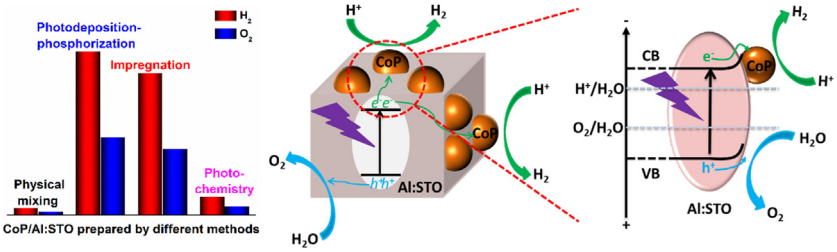

ARTICLE INFO

Article history:
Received 3 June 2021
Revised 29 July 2021
Accepted 7 August 2021
Available online 11 August 2021

Keywords:
Noble-metal-free
Overall water splitting
Metal phosphide
Perovskite
Photocatalysis

ABSTRACT

CoP, a noble-metal-free cocatalyst, was first introduced onto the surface of Al-doped $SrTiO_3$ (Al:STO) via an in situ photodeposition-phosphorization method for photocatalytic overall water splitting (POWS) into stoichiometric H_2 and O_2. Compared with pure Al:STO, the POWS activity was enhanced by a factor of ~ 421 over 1.0%CoP/Al:STO, with the highest evolution rates of 2106 and 1002 μmol h^{-1} g^{-1} for H_2 and O_2, respectively. The mechanism for the remarkably boosted POWS activity was systematically analyzed based on the comprehensive characterization. On the one hand, benefiting from the in situ photodeposition process, CoP with metallic character were intimately decorated onto the surface of Al:STO and accelerated the separation and migration of photoinduced charge carriers. On the other hand, CoP, serving as reactive sites for H_2 evolution reaction, lowered the overpotential and facilitated the surface reduction reaction, thereby enhancing the POWS activity. Furthermore, Cr_2O_3 was photodeposited on the surface of 1.0%CoP/Al:STO composite to suppress the undesired reverse reaction and the POWS activity was further enhanced up to 3558 and 1722 μmol h^{-1} g^{-1} for H_2 and O_2, respectively, with apparent quantum yield of 7.1% at 350 ± 10 nm. This work presents a new avenue for designing POWS system without noble-metal cocatalyst.

1. Introduction

Photocatalytic water splitting, as one of the most promising approaches to converting inexhaustible renewable solar energy into carbon-free hydrogen energy, has been extensively investigated over the past decades, and various of photocatalysts have been exploited, accordingly [1–4]. However, most photocatalysts could only be applied for either H_2 evolution reaction (HER) or O_2 evolution reaction (OER) in the presence of corresponding sacrificial reagents, which severely restrain their practical application [5–8]. Up to now, only a handful of photocatalysts have been reported to be capable of photocatalytic overall water splitting (POWS) with stoichiometric H_2 and O_2 production, such as

* Corresponding authors.
E-mail addresses: xj-guan@mail.xjtu.edu.cn (X. Guan), lj-guo@mail.xjtu.edu.cn (L. Guo).
[1] These authors contributed equally to this work.

https://doi.org/10.1016/j.jcis.2021.08.049
0021-9797/

La-doped $NaTaO_3$ [9], Ga(In)N [10,11], Al-doped $SrTiO_3$ (Al:STO) [12,13], $(Ga_{1-x}Zn_x)(N_{1-x}O_x)$ [14], $Ta_3N_5/KTaO_3$ [15], and $Y_2Ti_2O_5S_2$ [16]. Among them, oxide photocatalysts have received great attention owing to their merits of low cost, excellent stability, and high efficiency. Typically, Domen et al. applied Al:STO to POWS reaction for the first time and an apparent quantum yield (AQY) of 30% was obtained at 360 nm [12]. Recently, a record-breaking AQY of 95.9% at 360 nm for Al:STO was achieved by co-loading Rh/Cr_2O_3 and CoOOH [13]. However, it should be noted that the high efficiency of Al:STO, as well as other typical overall-water-splitting photocatalysts, greatly depend on the loading of noble-metal cocatalyst, which is economically unfavorable for potential large-scale application [11–13]. Therefore, it is urgently necessary to seek noble-metal-free cocatalysts for POWS.

Recently, transition metal phosphides (TMPs), such as CoP [17–19], Ni_2P [20], MoP [21], and Cu_3P [22], have been widely applied as cocatalysts for photocatalytic water splitting because of their low cost, high electrical conductivity, and polytropic composition. Among them, CoP has attracted the most attention as either HER or OER cocatalyst owing to its metallic character, Schottky effect, and chemical stability [19,23–25]. CoP as photocatalytic HER cocatalyst was first reported by Fu et al. in 2015, and the established CoP/CdS hybrid system exhibited excellent stability for>100 h in the company of sacrificial reagent [19]. In 2017, Wang et al. introduced CoP on g-C_3N_4 as oxidative cocatalyst for OER using $AgNO_3$ as electron scavenger [23]. Nevertheless, single CoP has been rarely applied as cocatalyst for POWS into stoichiometric H_2 and O_2. In addition, CoP as cocatalyst was generally loaded on photocatalysts by physical mixing [19], impregnation [23], and photochemistry methods [26], which usually gave birth to relatively loose contact between CoP and photocatalysts, thus resulting in unsatisfied performance. Therefore, it is of great significance to seek superior method to manufacture intimate contact heterojunction between CoP and photocatalysts.

Herein, CoP as noble-metal-free cocatalyst was attached intimately onto the surface of Al:STO via an in situ photodeposition-phosphorization method. The as-prepared CoP/Al:STO composites were employed for POWS into stoichiometric H_2 and O_2, and the mechanism of enhanced POWS was systematically investigated according to the comprehensive analysis based on various characterizations. This work may offer a new thought for the development of low cost POWS system.

2. Experimental section

2.1. Synthesis of photocatalysts

Al:STO was prepared by a flux method as model photocatalyst according to the previous report [12], and the detailed synthesis process was supplied in supporting information. CoP/Al:STO composites were prepared by an in situ photodeposition-phosphorization method, and the typical process was described detailly as follows.

For the in situ photodeposition process, 0.01 mmol $Co(NO_3)_2$ was dissolved in 150 mL deionized water, then 1 mmol Al:STO was added. The obtained dispersion was transferred into a 190 mL Pyrex glass reactor with a side window and purged with Ar for 10 min to eliminate air. Then the dispersion was irradiated from the side window using a 300 W Xe arc lamp at 35 °C under continuous stirring for the photodeposition of CoOOH onto the surface of Al:STO. After irradiated for 10 h, the dispersion was centrifuged and rinsed with deionized water for several times. The obtained product was dried at 60 °C under vacuum for 12 h and labeled as 1.0%CoOOH/Al:STO.

With regard to the phosphorization process, NaH_2PO_2 was chosen as the phosphorus source, which could generate phosphine during the calcination process. Typically, the collected 1.0% CoOOH/Al:STO and NaH_2PO_2 with a mass ratio of 1:5 were put into two sides of a crucible to avoid the direct contact between 1.0% CoOOH/Al:STO and NaH_2PO_2 as well as the potential P doping. To guarantee the sufficient phosphorization of CoOOH into CoP, the crucible was covered with a lid, transferred in a tube furnace, and heated at 300 °C for 2 h with a heating rate of 2 °C min^{-1} under an inert atmosphere of Ar flow. After naturally cooling to room temperature, the product was rinsed with deionized water and ethanol for several times to eliminate the possibly adsorbed PH_3 on the surface of photocatalyst, dried at 60 °C for 12 h under vacuum, and finally collected and labeled as 1.0%CoP/Al:STO. Samples with other contents of CoP were prepared based on the same process by adjusting the molar ratio of $Co(NO_3)_2$ and Al:STO, and the corresponding products were labeled as *x*CoP/Al:STO (*x* = 0.5, and 3.0%).

To exhibit the superiority of CoP/Al:STO composites prepared by the in situ photodeposition-phosphorization method, 1.0%CoP/Al:STO composites were also prepared by physical mixing, impregnation, and photochemistry methods for comparison, and the detailed synthesis process was supplied in supporting information.

2.2. Photocatalytic measurements

POWS reaction was conducted in a top-irradiated quartz reactor connected to a closed gas circulation system (LabSolar 6A, PerfectLight, Beijing). 20 mg of photocatalyst was uniformly suspended in 100 mL deionized water with stirring. After pumped to vacuum, the dispersion was irradiated by a 300 W Xe arc lamp and the temperature was maintained at ~ 298 K. The evolved H_2 and O_2 were analyzed by an online gas chromatograph with a 5A molecular sieve column, a thermal conductivity detector, using Ar as carrier gas. The AQY for POWS was measured under the above Xe arc lamp with a band-pass filter (λ = 350 nm), and calculated according to the following equation.

$$\mathrm{AQY}(\%) = \frac{\text{Number of reacted electrons}}{\text{Number of incident photons}} \times 100\%$$

$$= \frac{\text{Number of } H_2 \text{ evolved} \times 2}{\text{Number of incident photons}} \times 100\%$$

3. Results and discussion

3.1. Preparation process

Fig. 1 exhibits the facile synthetic route of CoP/Al:STO composites via a photodeposition-phosphorization method. Firstly, cobalt (hydr)oxide nanoparticles (marked by red circles) were tightly attached on the surface of Al:STO nanocubes via an in situ photodeposition method as the transmission electron microscopy (TEM) image exhibited (Fig. S1a). To identify the cobalt (hydr)oxide, high-resolution transmission electron microscopy (HRTEM) image was recorded and the lattice spacing with a distance of ca. 0.440 nm could be well indexed to the (003) plane of CoOOH (Fig. S1b) [27], demonstrating that the photodeposited cobalt (hydr)oxide was CoOOH, which is consitent with previous report [13]. Then PH_3 derived from the pyrolysis of NaH_2PO_2 could convert CoOOH to CoP through a phosphorization process. Considering that Al:STO was fabricated through a high temperature flux method at around 1100 °C, the phosphorization treatment at ~ 300 °C would scarcely affect the crystal structure and morphology of Al:STO.

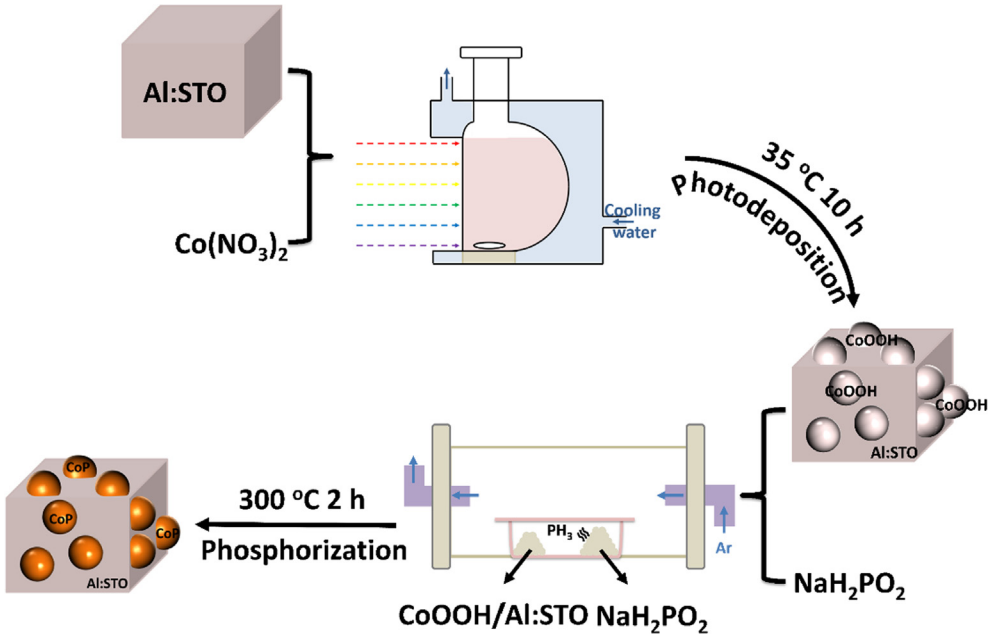

Fig. 1. Schematic illustration of the synthesis of CoP/Al:STO composites via a photodeposition-phosphorization method.

3.2. Microstructure and morphology characterization

Fig. 2, S2, and S3 demonstrate X-ray diffraction (XRD) patterns, scanning electron microscopy (SEM), TEM, and HRTEM images of the as-prepared samples. Bare Al:STO possessed a standard $SrTiO_3$ (JCPDS No. 00–035-0734) cubic phase perovskite structure (Fig. 2a) and cubic morphology with the size ranging from 100 nm to 1 μm (Fig. S3a), which was well matched with previous results [12], indicating the successful preparation of Al:STO. Upon loading CoP, the composites exhibited analogous XRD patterns and morphologies (Fig. 2 and S3), confirming that the as-proposed photodeposition-phosphorization process scarcely affected the microstructure and morphology of Al:STO. Moreover, no obvious shift could be observed for the strongest diffraction peak of Al:STO after the introduction of CoP (Fig. S2), thus eliminating the possibility of P doping. It should be pointed out that no characteristic peaks of CoP were observed for all CoP/Al:STO composites, which might be due to its relatively low content and weak crystallinity. However, it could be clearly observed that CoP nanoparticles (marked by red circles) were tightly attached on the surface of Al:STO as CoOOH, demonstrating that the intimate contanct between CoOOH and Al:STO originated from the in situ photodeposition process could be well maintained through phosphorization treatment (Fig. 2c). Furthermore, the lattice spacing with distances of ca. 0.276 nm, 0.247 nm, and 0.245 nm in HRTEM image could be well indexed to the (2 1 1) plane of Al:STO [28], (1 1 0) and (1 0 2) planes of CoP [24,29], respectively (Fig. 2d). Accordingly, CoP/Al:STO composites were successfully prepared by decorating CoP nanoparticles intimately on the surface of Al:STO nanocubes via a photodeposition-phosphorization method.

In addition, the Brunauer-Emmett-Teller (BET) surface areas for as-prepared samples were measured and listed in Table S1. For bare Al:STO, it exhibited the lowest BET surface area of 5.5 $m^2 g^{-1}$. With regard to the composites, the BET surface areas increased slightly with the loading amount of CoP, which could be ascribed to the ultrasmall particle size of CoP. However, it was worth noting that all samples possessed comparable BET surface areas, which was also supported by their analogous morphology as shown in Fig. S3, further implying that the photodeposition-phosphorization process had little effect on the microstructure and morphology of Al:STO.

3.3. Chemical composition and state

To investigate the surface chemical compositions of as-prepared samples, the X-ray photoelectron spectroscopy (XPS) survey scan spectra for Al:STO and 1.0%CoP/Al:STO samples were obtained and the results are shown in Fig. 3a. For bare Al:STO, only Sr, Ti, O and adsorbed C elements were detected, while 1.0%CoP/Al:STO composite revealed the signals of Co and P elements as well as Sr, Ti, O and adsorbed C elements, indicating that CoP was successfully introduced on the surface of Al:STO. It should be pointed out that Al element was diffcult to identify in the survey scan spectra for its low content. To disclose the surface chemical states of as-prepared samples, high-resolution XPS spectra were further measured. With regard to bare Al:STO, a weak peak located at ~ 74.4 eV was observed for Al 2p orbital (Fig. S4), which could be assigned to Al^{3+} [30], evidencing the existence and low content of Al element in Al:STO. In addition, the two split peaks at 457.9 and 463.5 eV were corresponding to the $2p_{3/2}$ and $2p_{1/2}$ orbitals of Ti^{4+} [31,32], while the peaks located at 132.5 and 134.2 eV were attributed to the $3d_{5/2}$ and $3d_{3/2}$ orbitals of Sr^{2+} [32]. After loading CoP, the binding energies of Ti^{4+} and Sr^{2+} exhibited a positive shift of 0.4 eV, indicating the potential electron-transfer from Al:STO to CoP [33,34]. It should be noted that Sr 3d orbital overlapped P 2p orbital. As shown in Fig. 3c, the peaks located at 132.9 and 134.6 eV were attributed to the $3d_{5/2}$ and $3d_{3/2}$ orbitals of Sr^{2+}, while the peak located at around 129.3 eV was ascribed to P-Co in CoP [35]. Additionally, high-resolution spectrum of Co $2p_{3/2}$ orbital for 1.0%CoP/Al:STO was provided (Fig. 3d). The peaks located at 778.1 eV could be attributed to Co-P bond in CoP, while the peak at 780.4 eV, as well as the satellite peak at 786.0 eV could be assigned to surface oxidized cobalt species [36,37].

The bulk elemental compositions of as-prepared samples were detected by energy dispersive X-ray spectroscopy (EDS) analysis and the results are listed in Table S2. It could be observed that all the samples possessed similar Sr:Ti:Al molar ratio, which indicated that the photodeposition-phosphorization process scarcely

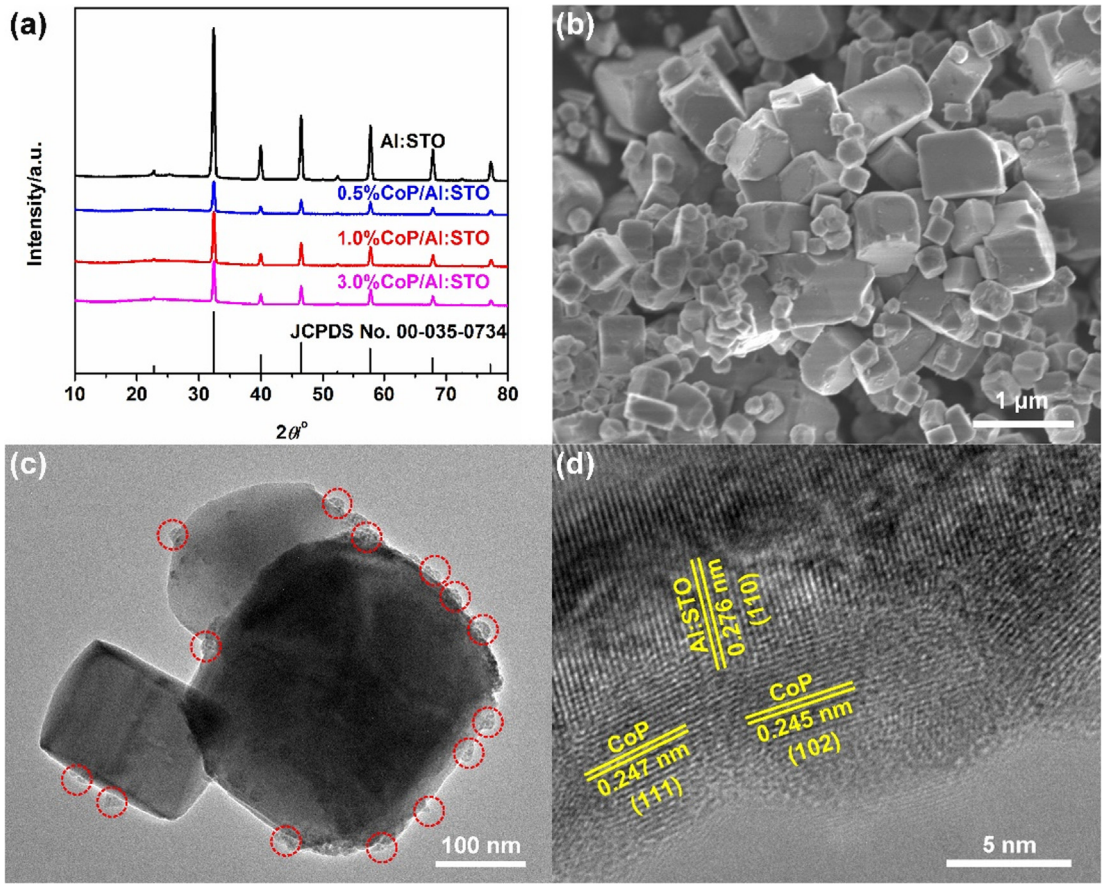

Fig. 2. (a) XRD patterns for as-prepared Al:STO and *x*CoP/Al:STO (*x* = 0.5, 1.0, and 3.0%) composites. (b) SEM, (c) TEM and (d) HRTEM images for 1.0%CoP/Al:STO.

affected the bulk elemental composition of Al:STO, thereby revealing the stable structure of Al:STO. To be specific, the Ti:Sr molar ratio was close to 100%, while the Al:Sr ratio was ~ 1.2%, implying the low content of Al element, which was in good agreement with the weak peak of Al 2p orbital aforementioned. As for the composites, the contents of Co and P was slightly lower than the feeding ratios, and increased with the loading amount of CoP. It should be noted that the molar ratio of Co:P was approximately 100%, further confirming chemical formula of CoP.

3.4. Optical properties

In addition, the XPS valance band for as-prepared Al:STO, 1.0% CoP/Al:STO, and CoP (Fig. S5) were measured as shown in Fig. 4a. It was observed that 1.0%CoP/Al:STO exhibited two valance band edges of 1.96 and −0.57 eV (vs. the Fermi level), which is in accordance with the valance band maximum (VBM) of Al:STO and CoP, respectively, thereby further confirming that CoP was successfully introduced onto the surface of Al:STO. It is worth noting that the VBM of CoP was lower than the Fermi level, demonstrating its metallic character [38], which could also be evidenced by its high absorption coefficient from ultraviolet to visible region as shown in Fig. 4b. As for Al:STO, it performed a 390 nm absorption edge corresponding to a band gap energy of ~ 3.19 eV. After loading CoP, the absorption in the visible light range was significantly increased with the loading amount of CoP. However, the absorption edges for the composites remained nearly the same with that of pure Al:STO, implying that CoP was loaded on the surface instead of introduced in the crystal lattice of Al:STO, which was consistent with the TEM results. Accordingly, CoP, with metallic character, was successfully introduced on the surface of Al:STO.

3.5. Photocatalytic performance

POWS of the as-prepared samples were conducted and the results are shown in Fig. 5. Bare Al:STO exhibited a very low H_2 evolution rate of ~ 5 μmol h^{-1} g^{-1} due to the less effective reactive sites. After loading CoP, the POWS activities of CoP/Al:STO composites were significantly enhanced (Fig. 5a). Specifically, the highest activity was achieved on 1.0%CoP/Al:STO, with gas evolution rates of 2106 and 1002 μmol h^{-1} g^{-1} for H_2 and O_2, respectively, which was ~ 421 times as those of bare Al:STO, corresponding to an AQY of 4.2% at 350 ± 10 nm (The detailed information for the calculation of AQY was supplied in Table S3). However, the POWS activity diminished when further increasing CoP amount because the absorption of Al:STO would be blocked by excessive CoP [21]. In addition, reports about CoP as single cocatalyst for photocatalytic water splitting in recent years were listed in Table S4. It could be found that CoP cocatalyst was generally applied for photocatalytic half reaction and there were few reports about single CoP as cocatalyst for POWS. Fortunately, single CoP was loaded on Al:STO in this manuscript and achieved the goal of decomposing water into stoichiometric H_2 and O_2.

To evaluate the photocatalytic stability of as-prepared CoP/Al:STO composites, cyclic tests were carried out. As shown in Fig. 5b, the gas evolution rates of 1.0%CoP/Al:STO revealed little decrease after 3 cyclic tests for 9 h, implying the excellent POWS stability of CoP/Al:STO composites prepared by the photodeposition-phosphorization method. In addition, the XRD

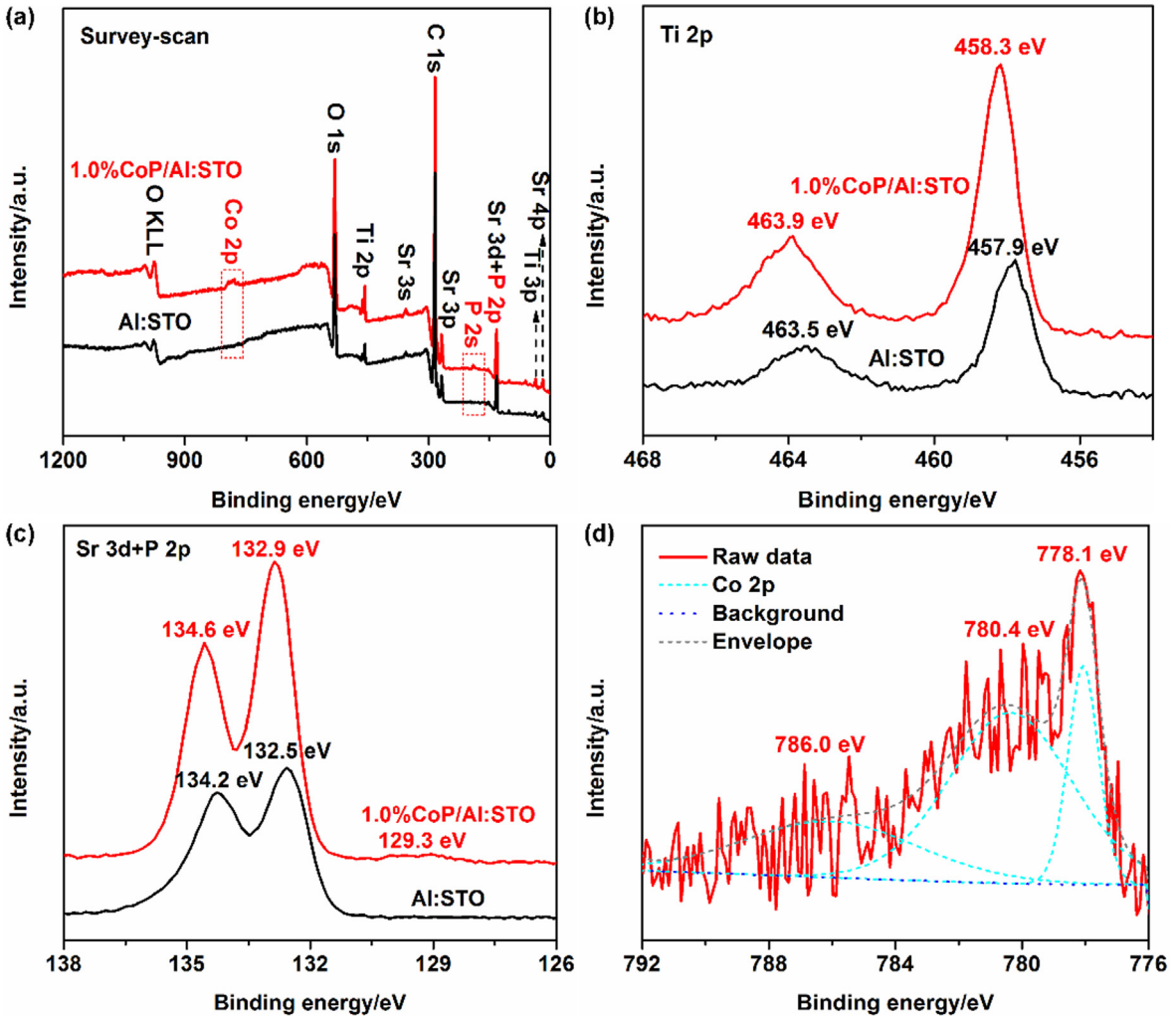

Fig. 3. (a) Survey-scan XPS spectra, high resolution XPS spectra of (b) Ti 2p and (c) Sr 3d + P 2p orbitals for Al:STO and 1.0%CoP/Al:STO. (d) High resolution XPS spectrum of Co $2p_{3/2}$ orbital for 1.0%CoP/Al:STO.

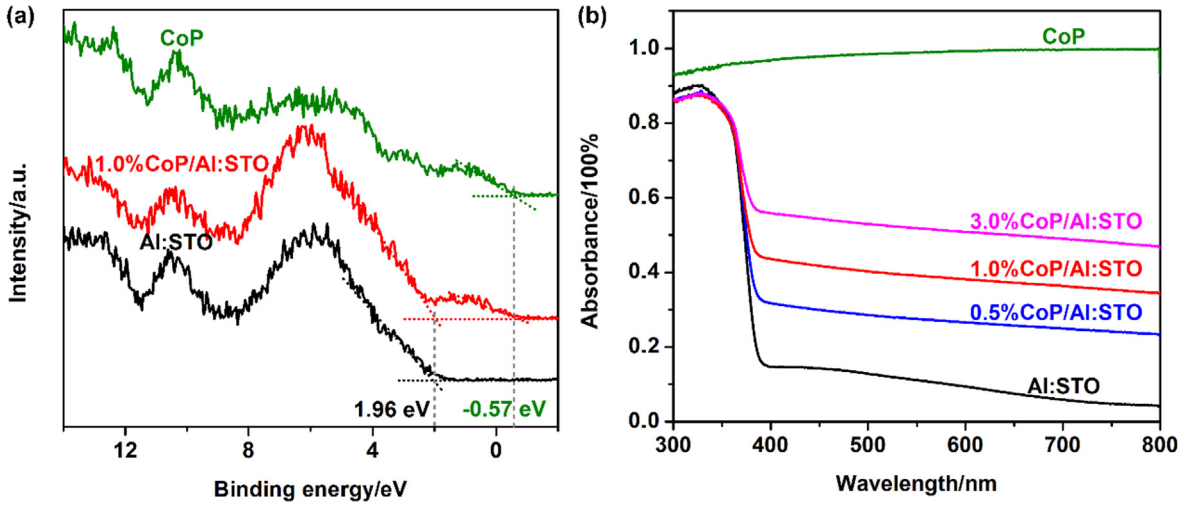

Fig. 4. (a) XPS valance band spectra for as-prepared Al:STO, 1.0%CoP/Al:STO, and CoP. (b) UV–vis spectra for as-prepared Al:STO, *x*CoP/Al:STO (*x* = 0.5, 1.0, and 3.0%) composites, and CoP.

patterns for 1.0%CoP/Al:STO kept almost the same before and after POWS (Fig. S6), which also indicated the stability of CoP/Al:STO composites. Furthermore, the TEM and HRTEM images for 1.0% CoP/Al:STO after POWS were obtained as shown in Fig. S7. It could be observed the CoP nanoparticles were still decorated intimately on the surface of Al:STO nanocubes after POWS, further confirming

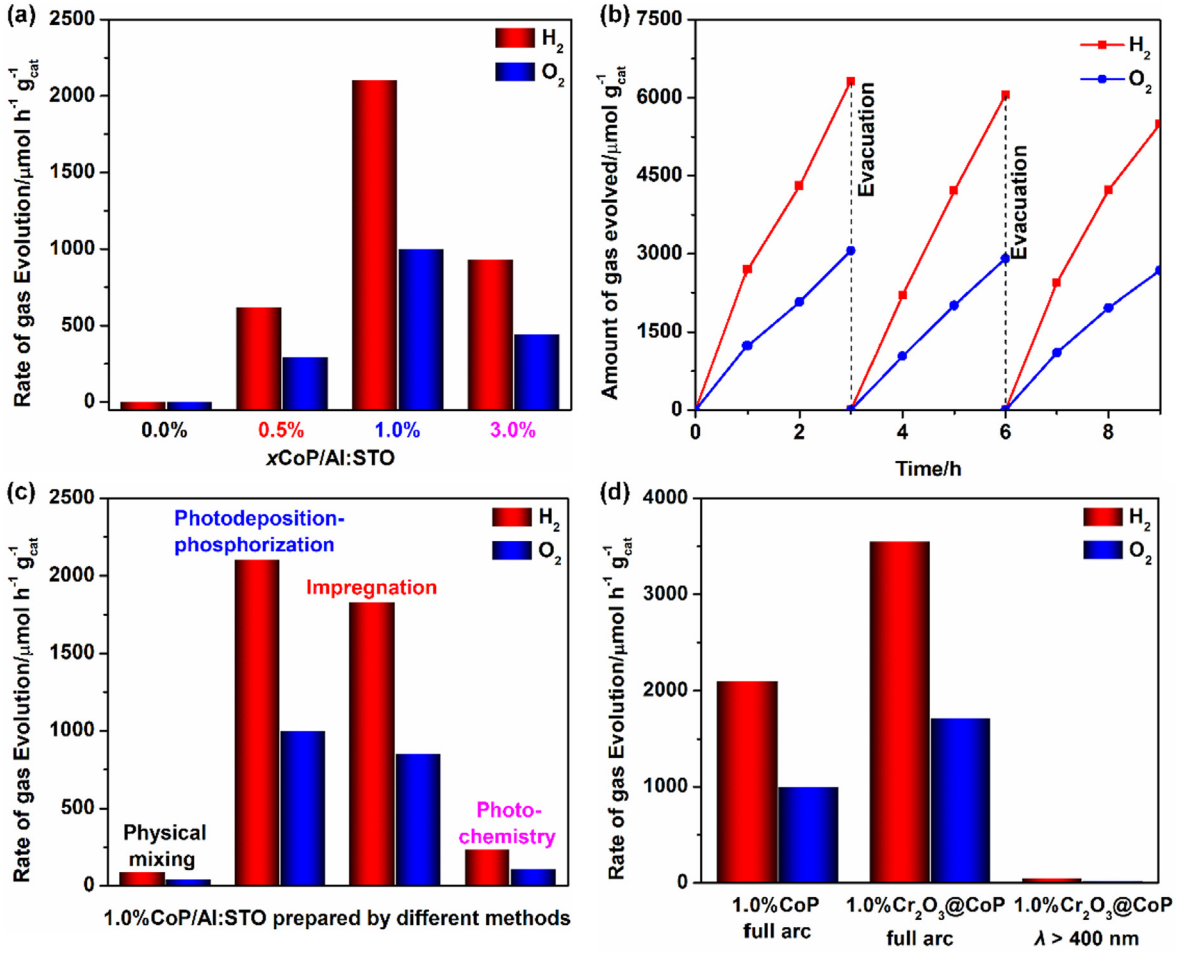

Fig. 5. (a) POWS performance for as-prepared Al:STO and *x*CoP/Al:STO (*x* = 0.5, 1.0, and 3.0%) composites under full-arc irradiation. (b) POWS stability tests of 1.0%CoP/Al:STO under full arc irradiation. (c) POWS performance for 1.0%CoP/Al:STO composites prepared by different methods under full arc irradiation. (d) POWS performance for 1.0%CoP/Al:STO and 1.0%Cr_2O_3@1.0%CoP/Al:STO under full arc and visible light (λ > 400 nm) irradiation.

the excellent stability of CoP/Al:STO composites prepared by the photodeposition-phosphorization method.

For comparison, the photocatalytic performance of 1.0%CoP/Al:STO samples prepared by physical mixing, impregnation and photochemistry methods was also investigated as shown in Fig. 5c. Compared with bare Al:STO, all the compisites exhibited enhanced photocatalytic performance, cofirming that CoP could indeed boost the POWS activity of Al:STO. Moreover, the composite prepared by the photodeposition-phosphorization method exhibited superior photocatalytic performance than the others prepared by physical mixing, impregnation and photochemistry methods, which usually gave birth to relatively loose contact between different components, thus demonstrating that the intimate contact between CoP and Al:STO resulting from the photodeposition-phosphorization process played a crucial role during the POWS. Specially, the composite by simply mixing CoP and Al:STO possessed the lowest gas evolution rates of about 91 and 44 μmol h^{-1} g^{-1} for H_2 and O_2, respectively, due to the worst contact between CoP and Al:STO.

In addition, to suppress the undesired reverse reaction [39], Cr_2O_3 was further in situ photodeposited on the surface of 1.0% CoP/Al:STO composite prepared by the photodeposition-phosphorization method. As shown in Fig. S8, the high resolution XPS spectrum of Cr 2p orbital exhibited two split peaks at 576.9 and 586.7 eV, which could be ascribed to $2p_{3/2}$ and $2p_{1/2}$ orbitals of Cr^{3+}, respectively [40], demonstrating that Cr_2O_3 was successfully photodeposited on the surface of 1.0%CoP/Al:STO. Compared with 1.0%CoP/Al:STO, the as-prepared 1.0%Cr_2O_3@1.0%CoP/Al:STO exhibited superior POWS activity with the gas evolution rates of 3558 and 1722 μmol h^{-1} g^{-1} for H_2 and O_2, respectively, with an AQY of 7.1% at 350 ± 10 nm. Moreover, the as-prepared 1.0% Cr_2O_3@1.0%CoP/Al:STO even exhibited POWS activity (52 μmol h^{-1} g^{-1} for H_2) under visible light (λ > 400 nm) irradiation.

3.6. Photocatalytic mechanism

Photoluminescence (PL) and Electrochemical impedance spectra (EIS) were carried out to disclose the separation and migration of charge carriers and the results are shown in Fig. 6a and S9. The fluorescence intensity of 1.0%CoP/Al:STO was much lower than that of bare Al:STO (Fig. 6a), implying that the loading of CoP could enhance the seperation and migration of photoinduced charge carriers and hence inhibit their internal recombination. Similarly, 1.0% CoP/Al:STO exhibited a smaller arc radius than bare Al:STO (EIS in Fig. S9), indicating that the charge transfer resistance could be effectively decreased after loading CoP, which was consistent with the results of PL spectra. Specially, electrochemical performance for Al:STO and 1.0%CoP/Al:STO were recorded, as shown in Fig. 6b. Compared with bare Al:STO, 1.0%CoP/Al:STO exhibited a positive-shift overpotential (with 0.12 V difference at 1 mA cm^{-2}), implying that CoP could significantly enhance the HER ability of Al:STO by serving as cocatalyst. In addition, photocatalytic H_2 evolution half reactions for Al:STO and 1.0%CoP/Al:STO were conducted

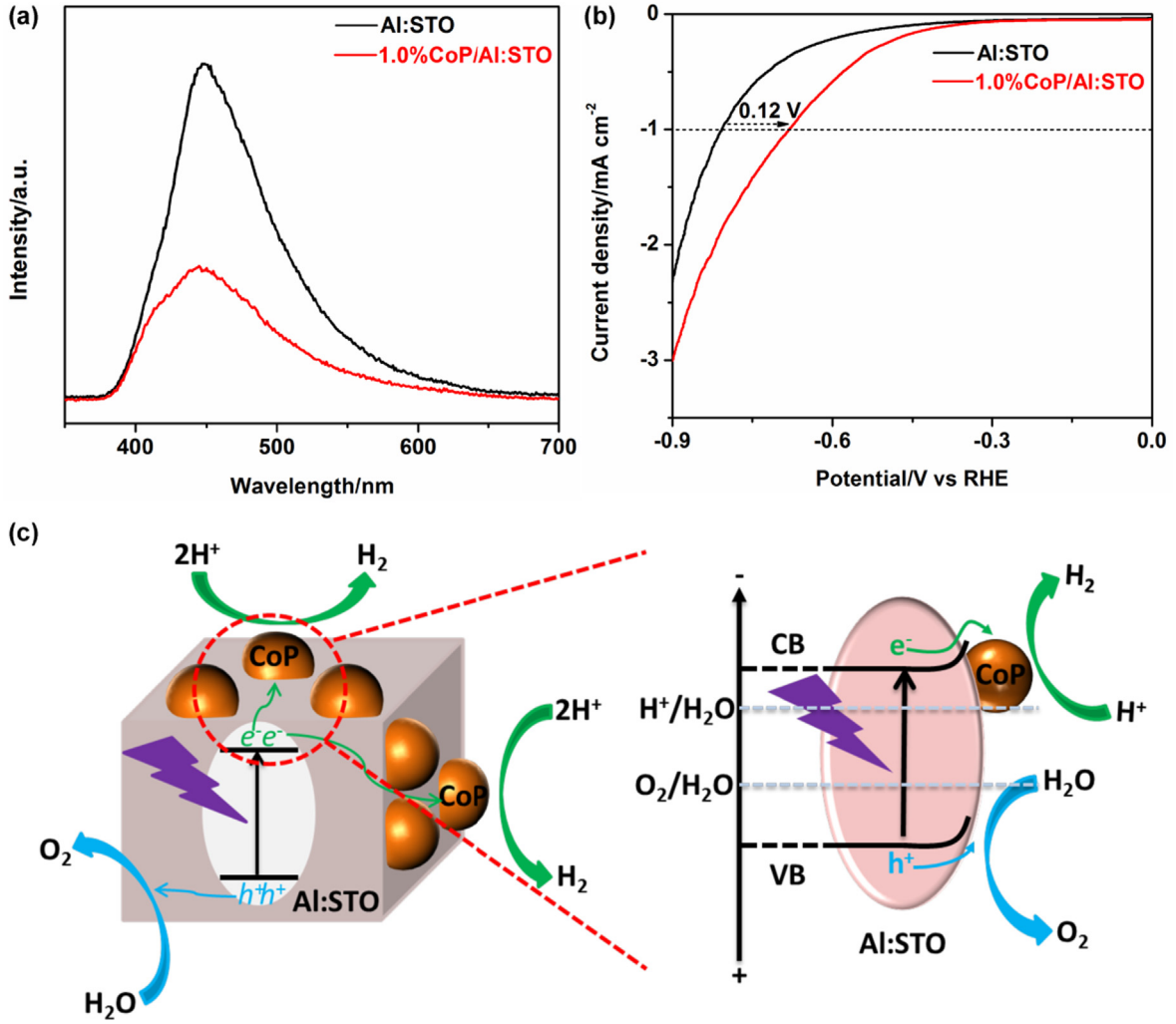

Fig. 6. (a) PL spectra, and (b) HER performance for Al:STO and 1.0%CoP/Al:STO composite. (c) Schematic illustration for the POWS of CoP/Al:STO composites.

as shown in Fig. S10. Compared with 1.0%CoP/Al:STO, bare Al:STO possessed negligible H_2 evolution, which also demonstrated that CoP functioned as HER cocatalyst. Moreover, photodeposition of Pt over 1.0%CoP/Al:STO was conducted, and the scanning transmission electron microscopy (STEM) image and corresponding elemental mapping images are exhibited in Fig. S11. It was observed that the distribution of Pt element was almost the same as that of P element, which further confirmed that the CoP on the surface of Al:STO served as the reduction reaction sites, i.e, active sites for H_2 evolution.

Based on the comprehensive characterizations and analysis, the mechanism for the boosted POWS performance was proposed and illustrated as Fig. 6c. On the one hand, CoP nanoparticles, decorated intimately on the surface of Al:STO nanocubes through the novel photodeposition-phosphorization process, possessed metallic character and should be responsible for the enhanced seperation and migration of photoinduced charge carriers [38]. On the other hand, CoP was able to lower the overpotential and decrease the energy barrier for H_2 production, enhancing the HER ability of Al:STO, thereby facilitating the POWS process significantly [24,36,41].

4. Conclusions

In conclusion, single noble-metal-free cocatalyst CoP was intimately decorated onto the surface of Al:STO via a novel in situ photodeposition-phosphorization method for POWS into stoichiometric H_2 and O_2. The introduced CoP, with metallic character, not only accelerated the separation and migration of photoinduced charge carriers, but also decreased the overpotential for H_2 production and facilitated the surface reduction reaction, thereby enhancing the POWS activity. Accordingly, the highest photocatalytic activities was obtained over 1.0%CoP/Al:STO, and the corresponding evolution rates for H_2 and O_2 reached 2106 and 1002 μmol h^{-1} g^{-1}, respectively, which was ~ 421 times higher than those of pure Al:STO. Benefiting from the intimate contact derived from the in situ photodeposition process, the CoP/Al:STO composite prepared by photodeposition-phosphorization method exhibited superior POWS activity than those prepared by conventional physical mixing, impregination, and photochemistry methods, which usually gave birth to relatively loose contact between CoP and Al:STO. Compared with previous reports [19,24,25,36,38], noble-metal-free cocatalyst CoP was first applied here as single cocatalyst on Al:STO for POWS into stoichiometric H_2 and O_2. Furthermore, Cr_2O_3 was photodeposited on the surface of 1.0%CoP/Al:STO composite to suppress the undesired reverse reaction and the POWS activity was further enhanced up to 3558 and 1722 μmol h^{-1} g^{-1} for H_2 and O_2, respectively, with an AQY of 7.1% at 350 ± 10 nm. It is believed that this work could provide a new avenue for designing POWS system without noble-metal cocatalyst. Future work is expected to proceed on decorating CoP with special morphology onto the surface of Al:STO for further enhanced POWS activity.

CRediT authorship contribution statement

Shichao Zong: Data curation, Formal analysis, Investigation, Writing – original draft. **Li Tian:** Formal analysis, Investigation, Writing – review & editing. **Xiangjiu Guan:** Conceptualization, Writing – review & editing, Supervision, Funding acquisition. **Cheng Cheng:** Writing – review & editing. **Jinwen Shi:** Writing – review & editing. **Liejin Guo:** Conceptualization, Writing – review & editing, Supervision, Funding acquisition.

Declaration of Competing Interest

The authors declare that they have no known competing financial interests or personal relationships that could have appeared to influence the work reported in this paper.

Acknowledgements

This work is supported by the Basic Science Center Program for Ordered Energy Conversion of the National Natural Science Foundation of China (No. 51888103). Xiangjiu Guan also would like to thank the finical support of the National Natural Science Foundation of China (No. 51906197), the Natural Science Foundation of Shaanxi Province (2020JQ-040), the China Postdoctoral Science Foundation (Nos. 2020 M673386, and 2020 T130503), and the Fundamental Research Funds for the Central Universities (xzy012019017).

Appendix A. Supplementary material

Supplementary data to this article can be found online at https://doi.org/10.1016/j.jcis.2021.08.049.

References

[1] Q. Wang, K. Domen, Particulate Photocatalysts for Light-Driven Water Splitting: Mechanisms, Challenges, and Design Strategies, Chem. Rev. 120 (2020) 919–985.
[2] L. Guo, Y. Chen, J. Su, M. Liu, Y. Liu, Obstacles of solar-powered photocatalytic water splitting for hydrogen production: A perspective from energy flow and mass flow, Energy 172 (2019) 1079–1086.
[3] Y. Wang, H. Suzuki, J. Xie, O. Tomita, D.J. Martin, M. Higashi, D. Kong, R. Abe, J. Tang, Mimicking Natural Photosynthesis: Solar to Renewable H_2 Fuel Synthesis by Z-Scheme Water Splitting Systems, Chem. Rev. 118 (2018) 5201–5241.
[4] X. Chen, S. Shen, L. Guo, S.S. Mao, Semiconductor-based Photocatalytic Hydrogen Generation, Chem. Rev. 110 (11) (2010) 6503–6570.
[5] Z. Wang, C. Li, K. Domen, Recent developments in heterogeneous photocatalysts for solar-driven overall water splitting, Chem. Soc. Rev. 48 (7) (2019) 2109–2125.
[6] S. Cao, T.-S. Chan, Y.-R. Lu, X. Shi, B. Fu, Z. Wu, H. Li, K. Liu, S. Alzuabi, P. Cheng, M. Liu, T. Li, X. Chen, L. Piao, Photocatalytic pure water splitting with high efficiency and value by Pt/porous brookite TiO_2 nanoflutes, Nano Energy 67 (2020) 104287.
[7] Z. Yi, J. Ye, N. Kikugawa, T. Kako, S. Ouyang, H. Stuart-Williams, H. Yang, J. Cao, W. Luo, Z. Li, Y. Liu, R.L. Withers, An orthophosphate semiconductor with photooxidation properties under visible-light irradiation, Nat. Mater. 9 (2010) 559–564.
[8] Y.-C. Chen, Y.-S. Huang, H. Huang, P.-J. Su, T.-P. Perng, L.-J. Chen, Photocatalytic enhancement of hydrogen production in water splitting under simulated solar light by band gap engineering and localized surface plasmon resonance of $Zn_xCd_{1-x}S$ nanowires decorated by Au nanoparticles, Nano Energy 67 (2020) 104225.
[9] H. Kato, K. Asakura, A. Kudo, Highly efficient water splitting into H_2 and O_2 over lanthanum-doped $NaTaO_3$ photocatalysts with high crystallinity and surface nanostructure, J. Am. Chem. Soc. 125 (10) (2003) 3082–3089.
[10] X. Guan, F.A. Chowdhury, Y. Wang, N. Pant, S. Vanka, M.L. Trudeau, L. Guo, L. Vayssieres, Z. Mi, Making of an Industry-Friendly Artificial Photosynthesis Device, ACS Energy Lett. 3 (9) (2018) 2230–2231.
[11] W. Fu, X. Guan, Z. Huang, M. Liu, L. Guo, Efficient photocatalytic overall water splitting over a core-shell GaInZnON@GaInON homojunction, Appl. Catal. B-Environ. 255 (2019) 117741.
[12] Y. Ham, T. Hisatomi, Y. Goto, Y. Moriya, Y. Sakata, A. Yamakata, J. Kubota, K. Domen, Flux-mediated doping of $SrTiO_3$ photocatalysts for efficient overall water splitting, J. Mater. Chem. A 4 (8) (2016) 3027–3033.
[13] T. Takata, J. Jiang, Y. Sakata, M. Nakabayashi, N. Shibata, V. Nandal, K. Seki, T. Hisatomi, K. Domen, Photocatalytic water splitting with a quantum efficiency of almost unity, Nature 581 (7809) (2020) 411–414.
[14] K. MAEDA, K. TERAMURA, K. DOMEN, Effect of post-calcination on photocatalytic activity of $(Ga_{1-x}Zn_x)(N_{1-x}O_x)$ solid solution for overall water splitting under visible light, J. Catal. 254 (2) (2008) 198–204.
[15] Z. Wang, Y. Inoue, T. Hisatomi, R. Ishikawa, Q. Wang, T. Takata, S. Chen, N. Shibata, Y. Ikuhara, K. Domen, Overall water splitting by Ta_3N_5 nanorod single crystals grown on the edges of $KTaO_3$ particles, Nat. Catal. 1 (10) (2018) 756–763.
[16] Q. Wang, M. Nakabayashi, T. Hisatomi, S. Sun, S. Akiyama, Z. Wang, Z. Pan, X. Xiao, T. Watanabe, T. Yamada, N. Shibata, T. Takata, K. Domen, Oxysulfide photocatalyst for visible-light-driven overall water splitting, Nat. Mater. 18 (8) (2019) 827–832.
[17] Y. Pei, Y. Cheng, J. Chen, W. Smith, P. Dong, P.M. Ajayan, M. Ye, J. Shen, Recent developments of transition metal phosphides as catalysts in the energy conversion field, J. Mater. Chem. A 6 (2018) 23220–23243.
[18] Y. Yang, C. Zhou, W. Wang, W. Xiong, G. Zeng, D. Huang, C. Zhang, B. Song, W. Xue, X. Li, Z. Wang, D. He, H. Luo, Z. Ouyang, Recent advances in application of transition metal phosphides for photocatalytic hydrogen production, Chem. Eng. J. 405 (2021) 126547.
[19] S. Cao, Y. Chen, C.-J. Wang, X.-J. Lv, W.-F. Fu, Spectacular photocatalytic hydrogen evolution using metal-phosphide/CdS hybrid catalysts under sunlight irradiation, Chem. Commun. 51 (41) (2015) 8708–8711.
[20] Z. Wang, Z. Jin, H. Yuan, G. Wang, B. Ma, Orderly-designed Ni_2P nanoparticles on g-C_3N_4 and UiO-66 for efficient solar water splitting, J. Colloid Interface Sci. 532 (2018) 287–299.
[21] C. Cheng, S. Zong, J. Shi, F. Xue, Y. Zhang, X. Guan, B. Zheng, J. Deng, L. Guo, Facile preparation of nanosized MoP as cocatalyst coupled with g-C_3N_4 by surface bonding state for enhanced photocatalytic hydrogen production, Appl. Catal. B-Environ. 265 (2020) 118620.
[22] R. Rameshbabu, P. Ravi, G. Pecchi, E.J. Delgado, R.V. Mangalaraja, M. Sathish, Black Trumpet Mushroom-like ZnS incorporated with Cu_3P: Noble metal free photocatalyst for superior photocatalytic H_2 production, J. Colloid Interface Sci. 590 (2021) 82–93.
[23] Z. Pan, Y. Zheng, F. Guo, P. Niu, X. Wang, Decorating CoP and Pt Nanoparticles on Graphitic Carbon Nitride Nanosheets to Promote Overall Water Splitting by Conjugated Polymers, Chemsuschem 10 (1) (2017) 87–90.
[24] B. Luo, R. Song, J. Geng, X. Liu, D. Jing, M. Wang, C. Cheng, Towards the prominent cocatalytic effect of ultra-small CoP particles anchored on g-C_3N_4 nanosheets for visible light driven photocatalytic H_2 Check tor production, Appl. Catal. B-Environ. 256 (2019) 117819.
[25] P. Tan, A. Zhu, Y.i. Liu, Y. Ma, W. Liu, H. Cui, J. Pan, Insights into the efficient charge separation and transfer efficiency of La, Cr-codoped $SrTiO_3$ modified with CoP as a noble-metal-free co-catalyst for superior visible-light driven photocatalytic hydrogen generation, Inorg. Chem. Front. 5 (3) (2018) 679–686.
[26] Y. Dong, L. Kong, G. Wang, P. Jiang, N.a. Zhao, H. Zhang, Photochemical synthesis of Co_xP as cocatalyst for boosting photocatalytic H_2 production via spatial charge separation, Appl. Catal. B-Environ. 211 (2017) 245–251.
[27] Z. Chen, C.X. Kronawitter, Y.-W. Yeh, X. Yang, P. Zhao, N. Yao, B.E. Koel, Activity of pure and transition metal-modified CoOOH for the oxygen evolution reaction in an alkaline medium, J. Mater. Chem. A 5 (2) (2017) 842–850.
[28] J. Wang, M. Kuo, P. Zeng, L. Xu, S. Chen, T. Peng, Few-layer $BiVO_4$ nanosheets decorated with $SrTiO_3$: Rh nanoparticles for highly efficient visible-light-driven overall water splitting, Appl. Catal. B-Environ. 279 (2020) 119377.
[29] D. Yang, W. Hou, Y. Lu, W. Zhang, Y. Chen, Cobalt phosphide nanoparticles supported within network of N-doped carbon nanotubes as a multifunctional and scalable electrocatalyst for water splitting, J. Energy Chem. 52 (2021) 130–138.
[30] T. Bala, G. Armstrong, F. Laffir, R. Thornton, Titania-silver and alumina-silver composite nanoparticles: Novel, versatile synthesis, reaction mechanism and potential antimicrobial application, J. Colloid Interface Sci. 356 (2011) 395–403.
[31] H. Bantawal, U.S. Shenoy, D.K. Bhat, Vanadium-Doped $SrTiO_3$ Nanocubes: Insight into role of vanadium in improving the photocatalytic activity, Appl. Surf. Sci. 513 (2020) 145858.
[32] D. Yang, Y. Sun, Z. Tong, Y. Nan, Z. Jiang, Fabrication of bimodal-pore $SrTiO_3$ microspheres with excellent photocatalytic performance for Cr(VI) reduction under simulated sunlight, J. Hazard. Mater. 312 (2016) 45–54.
[33] N. Boonprakob, N. Wetchakun, S. Phanichphant, D. Waxler, P. Sherrell, A. Nattestad, J. Chen, B. Inceesungvorn, Enhanced visible-light photocatalytic activity of g-C_3N_4/TiO_2 films, J. Colloid Interface Sci. 417 (2014) 402–409.
[34] J. Ran, W. Guo, H. Wang, B. Zhu, J. Yu, S.-Z. Qiao, Metal-Free 2D/2D Phosphorene/g-C_3N_4 Van der Waals Heterojunction for Highly Enhanced Visible-Light Photocatalytic H_2 Production, Adv. Mater. 30 (2018) 1800128.
[35] L. Han, T. Yu, W. Lei, W. Liu, K. Feng, Y. Ding, G. Jiang, P. Xu, Z. Chen, Nitrogen-doped carbon nanocones encapsulating with nickel-cobalt mixed phosphides for enhanced hydrogen evolution reaction, J. Mater. Chem. A 5 (32) (2017) 16568–16572.
[36] S. Cao, Y. Chen, H. Wang, J. Chen, X. Shi, H. Li, P. Cheng, X. Liu, M. Liu, L. Piao, Ultrasmall CoP Nanoparticles as Efficient Cocatalysts for Photocatalytic Formic Acid Dehydrogenation, Joule 2 (3) (2018) 549–557.
[37] Y. Fei, M. Liang, L. Yan, Y. Chen, H. Zou, Co/C@cellulose nanofiber aerogel derived from metal-organic frameworks for highly efficient electromagnetic interference shielding, Chem. Eng. J. 392 (2020) 124815.

[38] X.-J. Wang, X. Tian, Y.-J. Sun, J.-y. Zhu, F.-T. Li, H.-Y. Mu, J. Zhao, Enhanced Schottky effect of a 2D–2D CoP/g-C_3N_4 interface for boosting photocatalytic H_2 evolution, Nanoscale 10 (26) (2018) 12315–12321.

[39] K. Maeda, K. Teramura, D. Lu, N. Saito, Y. Inoue, K. Domen, Noble-metal/Cr_2O_3 core/shell nanoparticles as a cocatalyst for photocatalytic overall water splitting, Angew. Chem.-Int. Edit. 45 (46) (2006) 7806–7809.

[40] J. Chen, Z.-H. Lu, Q. Yao, G. Feng, Y. Luo, Complete dehydrogenation of $N_2H_4BH_3$ with NiM-Cr_2O_3 (M = Pt, Rh, and Ir) hybrid nanoparticles, J. Mater. Chem. A 6 (42) (2018) 20746–20752.

[41] S. Li, X. Hao, A. Abudula, G. Guan, Nanostructured Co-based bifunctional electrocatalysts for energy conversion and storage: current status and perspectives, J. Mater. Chem. A 7 (32) (2019) 18674–18707.